International Journal of Science and Research (IJSR)
ISSN: 2319-7064
ResearchGate Impact Factor (2018): 0.28 | SJIF (2018): 7.426

Local and Global Descriptors in CT Images for Efficient Pattern Classification

Dr Ibrahim M. Adekunle

Department of Information and Communication Technology, Osun State University, Osogbo, Nigeria

Abstract: ***Local and global features have recently attracted growing attention in the field of image processing and pattern recognition. The features from local binary pattern (LBP) for instance, usually lack global spatial information while global descriptors would provide very little local information. This paper develops two descriptors to tackle the existing problems in local and global features by providing more information to describe different textural structures in computed tomography (CT) images. The proposed global and local descriptors can provide more accurate classification results by using hybrid concatenation approach. The experimental procedures are validated for different scales of Emphysema images during the classification process in order to determine the appropriate image size that could yield the maximum classification accuracy. The experimental results show that the descriptors developed from the combined features considerably improve the performance of the classifiers. The results also indicate that the global descriptor outperforms the earlier approaches and demonstrate the discriminating power and robustness of the combined features for accurate classification of CT images.***

Keywords: Local Descriptor, Global Descriptor, Feature Extraction, Combined features, fractal dimension and classification accuracy

1. Introduction to Feature extraction

Features are the general information extracted from images or objects, which can be difficult to identify by human. When you consider image or object as data with certain dimension, features extraction would be of course smaller than the original image. This is simply because after preprocessing of images with image processing algorithms, some unwanted materials must have been eliminated while only useful information would be extracted as features and used for further experiments. This process would help us to focus on the important features in order to achieve accurate results since the inclusion of unwanted materials could make our experimental results to be erroneous. Additionally, processing of images or objects without feature extraction could increase the time and space complexity since the original image would occupy more memory and eventually consume more time than the reduced features with smaller dimensions. And that is why dimensional reduction is another stage in image processing, although, one must be very careful at this stage to ensure the important information are not being removed during this process. Some factors must be taken into consideration before you remove regions or parts of image. In computing, we can develop an algorithm or construct a model to achieve favourable results in this process.

There are two major types of features that can be extracted from images; local and global features. Global features are those features extracted from a complete image but when the same images are subdivided into various parts or sections or regions, the features extracted are called local features. Take for instance, image patches are smaller portions or fractional parts of the original image; I mean they are smaller in sizes and dimensions compared to the original size, features extracted in these patches can be referred to as local features. In other words, several smaller images can be obtained from one image, which means you can extract local features from global features during the classification process.

Global descriptors describe the general properties of the entire image but not to focus on a particular section or region. A very good example is the multi-fractal descriptors that was previously implemented and used in the analysis and classification of biomedical images by [7-12]. It is a global representation of shape, objects or images while local descriptors describe the image patches by focusing on certain regions within the images or shapes. Example of local descriptors can be found in local binary patterns (LBP). In this text, both descriptors would be used extensively in future for efficient analysis and classification of image patterns. This text also combines the features from local descriptors with that of global descriptors to generate new descriptors for further analysis and classification of biomedical images. Hopefully, hybrid concatenation of the features from both local and global descriptors could yield powerful features for efficient classification and analysis of images.

1.1 Techniques in Feature Extraction

Feature extraction technique involves processing of pixels or developing algorithms to manipulate pixels within images in order to detect or identify certain region. Basically in all digital images, arrangement of pixel gives useful information that could be used to process such image. For instance, in order to classify images, models could be developed to further refine or process the pixels for easy classification. In local binary patterns for instance, the algorithm is concern with the relationship between the centre pixel and its neighborhood. Various features can be derived or obtained from images but this depends on the model definition and how the pixel is processed. Most digital images have discrete pixels and this makes it easy for processing and manipulation to obtain discriminating features that can be used for classification, detection or identification. Pixel manipulation, arrangement or computation requires that one must be very good in Mathematics. The knowledge of mathematics can not be overemphasized in developing image processing algorithms. Features extracted within certain region of an image can be used to detect the characteristics that the entire image

possesses and this could be used in matching technique during recognition process. This technique would help the programmer or analyst to easily differentiate between closely related objects. Since you are not generally looking at the overview of images or objects, selecting small patches in an image would go a long way in helping us to identify the similarities and differences in images.

Transformation of pixels to another meaningful information using mathematical models that would allow further techniques such as machine learning, deep learning or even reinforcement learning involves feature extraction techniques. What you are trying to achieve would determine the methods or techniques you use for gathering information during this process. It is very important to study the data very well and probably visualize the contents of the object to understand how the data are arranged.

2. Computation of Local Features

The Higuchi's method is another efficient way of calculating the fractal dimension of a curve that has found several applications in the analysis of time series [6]. Higuchi's method is particularly suitable for a one-dimensional signal whose values at regular discrete intervals are available in the form $x(i)$, i = 1, 2, ...N. Several new data point series are constructed using an interval length, and starting value index t:

$$S_t(\varphi)=\{x(t), x(t+\varphi), x(t+2\varphi), \dots\dots x(t+p\varphi)\} \quad (1\text{-}1)$$

Where

$$p = [\tfrac{t-1}{\varphi}] \quad (1\text{-}2)$$

The length of the series in (1-4) is calculated as a normalized sum of differences:

$$l_r(\varphi)=\tfrac{N-1}{p\varphi^2}\sum_{i1}^{p} I\, x(t+i\varphi)-x(t+(i-1)\varphi) \quad (1\text{-}3)$$

The mean length for each interval length is obtained as

$$L(\varphi) = \frac{1}{\varphi}\sum_{\varphi}^{1} L_k(\varphi) \quad (1-4)$$

As in the case of the box-counting dimension, the Higuchi dimension D_H is also computed as the slope of a linear regression line obtained using a log-log plot with log(φ) along the x-axis, and log (L(φ)) along the y-axis.

An MxM image $I(x, y)$ must be converted to one-dimensional data before the above method can be applied. A common approach used for this is to add the values along each column to get a one-dimensional array of sums of pixel intensities:

$$x(x) = \textstyle\sum_{y=1}^{M} I(x,y), j = 1,2,\dots M. \quad (1\text{-}5)$$

2.1 Generalized Renyi Dimension

The box-counting dimension outlined above can be extended to a generalized family of dimensions called Renyi dimensions. These dimensions use a probability measure functionμ. In the context of the box- counting algorithm, μ_i represents the probability of finding a point of the fractal within a box with index i. The Renyi dimensions D_q are defined with respect to a non-negative parameter q as

$$D_q = \frac{1}{q-1}\lim_{\delta\to 0}\frac{\log_2[\sum_{i=1}^{N}\mu_i^q]}{\log_2\delta} \quad (1\text{-}6)$$

As a special case of the above, when q becomes 0, we get the box counting dimension. In a fractal system the measured object is assumed to have an internal structure with different spatial scales; the number N(e) of features of certain size e scale as [14], [20].

$$N(e)\sim e^{F} \quad (1\text{-}7)$$

Where F is the fractal dimension, which describes the scaling properties or the size distribution of 2D objects. The box counting method is used to obtain the scaling properties of the object by covering the measured object with boxes of size S and counting the number of boxes containing at least one pixel representing the object under study, N(S):

$$F_0 = \lim_{s\to 0}\frac{\log N(s)}{\log(\frac{1}{s})} \quad (1\text{-}8)$$

The box counting dimension F_0 can be determined as the slope of the linear regression of log N(S) versus log (1/s) measured over a range of box sizes. The multi-fractal measure can be characterized through the scaling of the kth moments of Pi distribution in the form [3], [14], [18].

$$\Sigma_{i=1}^{N(S)} P_i^k(S) = S^{(k-1)F_k} \quad (1\text{-}9)$$

where F_k is the generalized fractal dimension defined from Eq. (1-10) as:

$$F_k = \lim_{s\to 0}\frac{1}{k-1}\frac{\log\sum_{i=1}^{N(s)} p_i^k(s)}{\log s} \quad (1\text{-}10)$$

The exponent in Eq. (1-9) is known as the mass exponent of the kth order moment τ(q) [14], [16]:

$$\tau(k) = (k-1)F_k \quad (1\text{-}11)$$

As can be seen in Eq. (1-13), when k =0, all the boxes have a weight unity [1], [15], the numerator becomes N(S) and the F_k becomes the capacity dimension, F_0 (Eq. (1-11). The other two special cases are when k = 1 and k =2 which are known as the information dimension F_1 and correlation dimension F_2 respectively. For k = 1, it can be derived from Eq. (1-10) as:

$$F_1 = \lim_{s\to 0}\frac{\log\sum_{i=1}^{N(s)} pi\log pi}{\log s} \quad (1\text{-}12)$$

F_1 is directly related to the information or Shannon entropy [19], [24], which quantifies the degree of disorder present in a distribution. For k = 2 the correlation dimension F_2 can be obtained as:

$$F_2 = \lim_{s\to 0}\frac{\log\sum_{i=1}^{N(s)} pi^2}{\log s} \quad (1\text{-}13)$$

F2 is mathematically associated with the correlation function and computes the correlation of measures contained in intervals of size S. The fractal dimension of higher moments can be estimated according to Eq. (1-10). The Renyi spectrum is generated by the graphs of F_k versus k and it represents the mass distribution of an image. F_k addresses how mass varies with the e (resolution or box size) in an image. On the other hand, the plot of Fk for different values of k is called the generalized dimensional $F_2 \le F_1 \le F_0$, where the equality $F_0=F_1=F_2$ occurs only when the fractal is statistically or exactly self-similar and homogenous [23],

[26]. According to [1-10], the singularity spectrum can be calculated using a set of real numbers k by

$$\alpha(\mathrm{k}) = \lim_{s\to 0} \frac{\log \sum_{i=1}^{N(s)} \mu_i \log [pi(s)]}{\log s} \qquad (1\text{-}14)$$

and the direct computation of $f(\alpha_k)$ value is :

$$\mathrm{f}(\alpha_\mathrm{k}) = \lim_{s\to 0} \frac{\log \sum_{i=1}^{N(s)} \mu_{i(k,s)} \log [\mu i(k,s)]}{\log s} \qquad (1\text{-}15)$$

Where the quantities $\mu_i(k,s)$ are defined as

$$\mu_i(k,s) = \frac{p_i^k(s)}{\sum_{i=1}^{N(s)} p_i^k(s)} \qquad (1\text{-}16)$$

$p_i(S)$ is the fraction or probability of the object contained in each ith box of size S.

3. Implementation of Global features

In this section, we give an overview of the computational stages in the multi-fractal analysis of images. Even though these stages have already been described in the previous sections, the purpose of this section is to give an integrated view of the whole pipeline, showing the sequence of processes that should be implemented. In Figure 3-1, we provide a diagram of this processing pipeline consisting of three layers: the input layer, the computational layer and the output layer.

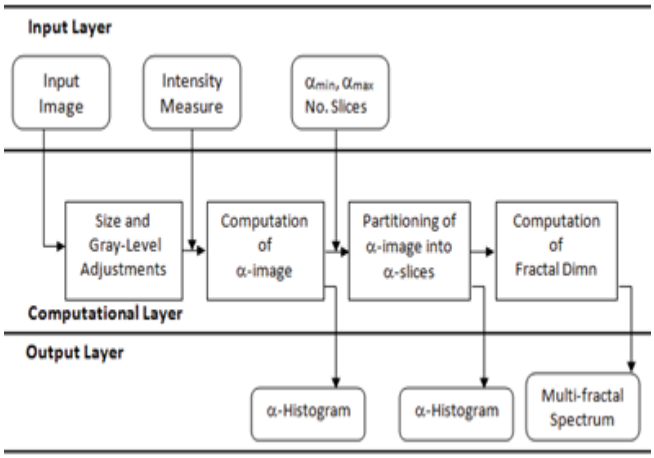

Figure 3-1: The main steps in the computation of multi-fractal spectrum of an input image

Note that the output layer includes two types of a-histograms. The first a- histogram is obtained directly from the α-image, where each α value is transformed into the range [0-255] and represented as a gray-level. The second α-histogram is obtained by discretizing the a-range [α_{min}, α_{max}] into *n* number of subintervals, and counting the number of pixels having α values in each subinterval.

3.1 Exact and Statistical Self-Similarity

The most important geometrical characteristic exhibited by fractals is self- similarity, which is the property of invariance under certain scale transformations. A fractal on a plane can be viewed as a bounded set *S* of two-dimensional points. The set *S* is self-similar if it is the union of *N* non-overlapping subsets, each of which is congruent to scaled versions of [13]. Two sets of points are congruent if by using a similarity transformation consisting of scaling, rotations, transformations and reflections; one set can be transformed into an exact copy of the other.

All real-world examples modelled using random fractals have statistical self-similarity. Here, different parts of a fractal cannot be made exactly congruent to the whole set even after an arbitrary rotational transformation and displacement. In this context, statistical self-similarity refers to the fact that enlargements of small constituent segments of a fractal have the same statistical distribution as the whole set [4].In other words, parts of a random fractal can be matched with the whole set only in a statistical sense. In a broader context, statistical self-similarity refers to the characteristic of having a nearly constant measurement (within an allowable threshold) of certain statistical parameters derived from sets at various scales.

The intensity distribution in lung tissue images is highly irregular and does not often permit a direct definition of shape parameters using geometrical descriptors. One approach towards extracting relevant features is to make use of the statistical self-similarities in local intensity variations. Most biomedical images exhibit such statistical self-similarity, a repetition of form over a variety of scales. Several methods of multi-fractal analysis of medical images have been suggested and evaluated in different ways [5], [17][22], [25]. [5] developed two-pass algorithm for the computation of multi-fractal spectrum and used the calculated spectra for the classification in a tissue image database. In [8], the holder exponent for the power law approximation of intensity measures in pixel neighbourhoods is used for resolving local density variations in the CT lung images.

4. Results and Discussion

In order to evaluate the discriminating capability of the combined features from the two descriptors, different classification experiments are conducted. Three Emphysema classes are defined with 50 images, assigned to each class. A comparison is made between the global descriptor and the result obtained from the recently published journal. We employ two different image classifiers due to the nature of the datasets used in this study; the SVM, and random forests (RF) [2]. The RF could be a perfect classifier for the multi-fractal datasets since it is relatively robust to outliers and noise, and always enhance better accuracy when random features are used. The RF randomly selects inputs or a combination of inputs to grow each tree. This can significantly improve the classification accuracy by combining trees grown using random features, and the generalization error of the forests reduces as the number of trees becomes large [2]. SVMs have demonstrated highly competitive performance in many real-world applications, such as bioinformatics, face recognition and image processing. [27] designed a biased maximum margin analysis and semi-supervised biased maximum margin analysis combined with the SVM to improve the performance of the traditional SVM as a relevance feedback for content based image retrieval (CBIR). In [27], a novel algorithm for subspace learning technique was also developed using SVM to exploit the user historical feedback

log data for a CBIR. Approximately 70% of the entire data set is used to train different SVM classifiers and 30% of the data sets generated are used for the testing. The results indicate that the global feature presents good classification performance, particularly with the RF classifier, though; the results obtained from the SVM are also good for the global features. As can be seen in Figure 4-1, It is noted from the results that the effects of the window size on the data sets are very obvious.

Table 4-1: Classification Results of the Global Descriptor

Classification accuracy – Global Feature		
Image Sizes	*SVM*	*Random Forest*
64 * 64	50.04%	73.17%
128 * 128	52.08%	81.52%
256 * 256	62.53%	92.45%
320 * 320	61.16%	94.38%
384 * 384	62.23%	96.13
512 * 512	60.51%	98.23%

In other words, the data sets with the largest image sizes gave the best classification accuracy, using two different classifiers while the data sets with the smallest image pixel size gave the lowest performance. These results also demonstrate that as the image size is increasing the overall classification accuracy is also increasing, which indicates that the larger the window size, the higher the classification accuracy. This is simply because the images with the larger sizes have captured more useful information, which eventually increase the discriminating power of the features used in the classification process. The original size of the patches does not contain enough discriminative information, which led to the reduction in the performance accuracy of the classification system. Overall, the performance of the global descriptor looks very good as the classification accuracy falls within the range of 73.17-98.23%. The scale invariance in the Emphysema images has really influenced the performance of the classification system, though, 512*512 resolution size is the maximum that we have tested with this descriptor. The performance of the classification system that uses 512*512 pixels has been impressive with an accuracy of 98.23%, even with big data sets, which are about 76800*1024 pixels after the concatenation. Probably, a further increase in the image window sizes might produce worse or better classification accuracy, but of course a classification accuracy of 98.23% is an excellent result. Generally, the RF classifier performed better than the SVM in all the cases, since the classification accuracy of the SVM classifier falls within the range of 50.04–60.51%. The local descriptor approach slightly affects the performances of the SVM classifier, but it is not as prominent as it does in the RF approach. The poor performances of the SVM classifier might be because it has not been trained with enough data sets, reducing the testing sets and increasing the training sets could probably increase the performances of the classifiers. The second descriptor that uses the local features and the α-images would be experimentally analyzed with the same procedures as the global descriptor. The classification results of the local descriptor using different image sizes with two different image classifiers are presented in Table 4-2.

Table 4-2: Classification Results of Local Descriptor

Classification accuracy – Local Descriptor		
Image Sizes	*SVM*	*Random Forest*
64 * 64	47.34%	56.78%
128 * 128	48.25%	47.67%
256 * 256	49.89%	46.11%

Performances of the local descriptor are generally lower than that of the global descriptor. Similarly, the scale invariance of different patch sizes does not have any significant impact on the classification accuracy. However, in the global descriptor, the effect of the window sizes of the patches is very obvious, this is expected because the data sets from the local descriptor do not really require further invariance examination as this has been done during implementation. Overall, the results are not really bad, but the global descriptor outperforms the local descriptor in terms of classification accuracy. Since the changes in the scale invariance to the corresponding results of the classification are not so obvious, the maximum image size tested during the experiment is therefore 256*256. The features derived from the local descriptor have higher discriminative power than the features obtained from the local descriptor. The second experiment compares the results from the global descriptor with the state of the art article (Sorensen, 2010). The confusion matrix with the best classification accuracy, which uses the global descriptor with the image size of 512*512 pixels, is presented in Table 4-1 for comparison with the state of the art paper for Emphysema classification [21]. As can be seen in Table 4-3, our results compare favourably with the LBP results; the overall accuracy of 98.53% from the confusion matrix obtained from the Emphysema image analysis compared to the accuracy of 95.2% that was achieved by LBP showed that the performance of the proposed descriptor is better in spite of a large volume of data sets. Additionally, our approach is simpler and faster in terms of time complexity. It has been verified experimentally that the execution run time to generate the global features is about 5 times faster than the time it would take to calculate LBP features using the same image size. Take for instance, for a 128*128 pixel size, the regular LBP run time was around 4.3s whereas it took just 0.9s to generate the global image of the same image size. Similarly, for a 512 * 512, the execution run time for the regular LBP was around 51.74s while both local and global features can be calculated in just 9.2s. The experimental tests for the time complexities were carried out for four different image sizes; that is; 64*64, 128*128, 256*256 and 512*512 for comparison between the regular LBP and the global image features. Generally, the LBP consumes more computational time than the global image. This can be very important, especially when dealing with a very large volume of data sets like 512*512 during classifications, which are around 76800*1024 pixels. The details of the computational time for both feature descriptors are presented in Table 4-4 using different image patches. The framework of this study provided solutions to few research questions in the field of image classifications. For instance, how does the feature extracted from the combination of LBP and multi-fractal descriptors behave under the same scale changes? Which of these features is dominant over the other? How does the descriptor generally compare with the related previous work using other textural classification approaches? It has been

demonstrated in this research work the effectiveness of the combined features derived from both LBP and the global descriptors in the classification of the Emphysema images. In the experimental analysis, we could see how powerful this descriptor is and how it behaves under different scale changes.

Table 4-4: Computational Time Comparisons between the Global Image and the Regular LBP

Computational Time in seconds		
Image size	*Global image*	*Local Image*
64 *64	0.3217s	1.3431s
128 *128	0.9113s	4.304s
256 * 256	2.3865s	11.15s
512 * 512	9.9017s	51.74s

Although, the global image and the local features have shown to be more powerful or more discriminating than the other features from the LBP and RILBP as this was verified during different experiments. This explains the importance of global features obtained from the multi-fractal descriptors compared to the local features from the LBP and the combined features from both descriptors, which also behave well under different scale changes.

5. Conclusions

In this study, we have analyzed the effect of different scale invariants on the Emphysema image classification using two different descriptors. We have shown that the proposed descriptors could perform well even with big data sets, especially the global descriptor that has really shown excellent performances in all cases. This is a great achievement as the classification of large data sets involved in this experiment may sometimes pose some challenges that may affect the performances of the classification system. But, in this case, as the data sets increases, the classification accuracy increases until the algorithm converges. The two descriptors proposed; the global and the local descriptors were defined to extract the textural characteristics of the images combined with the global properties for the classification of the images. We have also demonstrated using the global descriptors that the window sizes of the image have great influence on the classification accuracy. The combined feature that uses the global descriptor is better than the other descriptor (local). Likewise, the fusing of the LBP and global either in a joint or hybrid form produced a very good performance with overall classification accuracy of 98.53%. Global descriptor also outperforms the results obtained from the state-of-the-art paper by [17], which demonstrated the effectiveness and robustness of the proposed descriptor. The classification result that uses the original image scale (64*64) from the Emphysema database indicate that, the global descriptor achieves 75.16% using the RF classifier while the local descriptor reaches only 52.08%. This demonstrates that even before applying the scale invariances, global descriptor outperforms the local descriptors, which shows that the features from global possess better discriminating power than the features from local descriptor. Additionally, the scale invariance changes in patches do not have any significant changes in the classification accuracy in the local descriptor, but in the global, an increase in the scale of the patches further increases the classification accuracy. This proves that the changes in the scale invariance of the Emphysema patches further increase the discriminating capability of the features in the global descriptor. This is an indication that the features extracted from the global descriptor cope well with the scale changes, but the features from the local did not really do well with the scale changes in the image patches. Also, the performance of the RF classifier outperforms the SVM in all cases, though this improvement is not much in the local features since the classification accuracy has a range of 40-60%, but this improvement can be seen in the global descriptor as the accuracy increases from 50-60% in SVM to 75-99% in RF under different scale changes. One of the limitations in this research framework is that the local features did not combine well with the alpha image features and that can be seen in the performances of the descriptor during the classification process. Also in global descriptor, an increase in the data sets keeps increasing the classification accuracy, but also demanding more memory usage and the processor computational time. In order to improve the performances of the local descriptor, changes in the parameters like the number of neighbours, radius of pixels and even the angle of rotating the LBP when calculating the RILBP might provide better results.

References

[1] Appleby, S. (1996). Pattern of the Human Population. *Geographical Anaysis*, *28*(2), 147–160.
[2] Breiman, L. (2001). Random forests. *Machine Learning*, *45*, 5–32. doi:10.1023/A:1010933404324
[3] Chhabra, A., & Jensen, R. V. (1989). Physical Review letters. *Direct Determination of the F(alpha) Singularity Spectrum*, *62*(March), 1327– 1330.
[4] Falconer, K. (2003). Fractal Geometry- Mathematical Foundations and Applications. (2nd ed.). London: Wiley
[5] Hemsley, A., & Mukundan, R. (2009). Multifractal Measures for Tissue Image Classification and Retrieval. *llth IEEE International Symposium on Multimedia*, 618–623. doi:10.1109/ISM.2009.94\
[6] Higuchi, T. (1988). North-Holland Physics Publishing Division. *Physical D 3l*, 277–283.\
[7] Ibrahim, M., & Mukundan, R. (2014). Multifractal Techniques for Emphysema Classification in Lung Tissue Images. *International Proceedings of Chemical, Biological & Environmental Engineering*, *78*, 115–119. Retrieved from http://www.etlibrary.org/?m=fbook&a=details&aid=15734
[8] Ibrahim, M., & Mukundan, R. (2015). Cascaded techniques for improving emphysema classification in computed tomography images. *Artificial Intelligence Research*, *4*(2), 112–118. doi:10.5430/air.v4n2p112
[9] Ibrahim M.A., Ojo O.A., Oluwafisoye P.A. (2017). On Feature Selection Methods for Accurate Classification and Analysis of Emphysema CT Images. *International Journal of Medical Imaging*, *SciencePG* 5(6), 2017, 70-78. http://www.sciencepublishinggroup.com/journal/paperinfo?journalid=15 6&doi=10.11648/j.ijmi.20170506.12
[10] Ibrahim M.A., Ojo O.A., Oluwafisoye P.A.(2017). Analysis of Emphysema Patterns Computed

Tomography Image, *International Journal of Scientific & Engineering Research*, 8(12), 2157-2168. https://www.ijser.org/research-paper-publishing-december- 2017_page6.aspx

[11] Ibrahim M.A., Ojo O.A, P.A. Oluwafisoye P.A. (2018). Identification of Emphysema Patterns in High Resolution Computed Tomography Images. *Journal of Biomedical Engineering and Informatics* (Canada, 2017), Sciedupress 4(1), 16-24, 2018.

[12] Ibrahim M.A., Ojo O.A. "New Multi-fractal Techniques for Pattern Analysis in Biomedical Images", *SIA OmniSciptum Publishing, Latvia(2018), European Union;LAMBERT Academic Publishing: ISBN:978613989296-9.* https://www.omniscriptum.com

[13] Mandelbrot, B. B. (1977). *The Fractal Geometry of Nature*. New York:

[14] Martinez, F. S. J., Martin, M. A., Caniego, F. J., Tuller, M., Guber, A., & Pachepsky, Y. (1999). Multi fractal analysis of discretized X-ray CT images for the characterization of soil macropore structures.*Geoderma*, *l56*(2), 32-42.

[15] Mendoza, C. S., Washko, G. R., Ross, J. C., Diaz, A. A., Lynch, D. A., & Crapo, J. D. (2012). Emphysema Quantification in A Multi-Scanner HRCT Cohort using Local Intensity Distributions. *IEEE International Symposium on Biomedical Imaging*, 474–477.

[16] Miranda, J. G. V, Montero, E., Alves, M. C., González, A. P., & Vázquez, E. V. (2006). Multifractal characterization of saprolite particle-size distributions after topsoil removal. *Elsevier*, *l34*, 373–385. doi:10.1016/j.geoderma.2006.03.014

[17] Nilsson, E. (2007). Multifractal-based Image Analysis with applications in Medical Imaging. Department of Computer Science, Umea University, Umea Sweden.

[18] Oiwa, N., & Fiedler-Ferrara, N. (1998). Physical D. *Elsevier*, *l24*, 210– 224.

[19] Oudjemia, S., Girault, J., Derguini, N., & Haddab, S. (2013). Multifractal Analysis: Application to Medical Imaging., 244–249.

[20] Posadas, A. N. D., Giménez, D., Quiroz, R., & Protz, R. (2003). Multifractal Characterization Of Soil Pore Systems. *Journal of Food Engineering*, *67*, 1–14.

[21] Sørensen, L., Shaker, S. B., & Bruijne, M. De. (2010). Quantitative Analysis of Pulmonary Emphysema using Local Binary Patterns. *IEEE Transactions on Medical Imaging*, *29*(2), 559–569. doi:10.1109/TMI.2009.2038575

[22] Stojis, T., Reljin, I., & Reljin, B. (2006). Adaptation of multifractal analysis to segmentation of microcalcifications in digital mammograms. *Physica A: Statistical Mechanics and Its Applications*, *367*, 494–508. doi:S0378437105012331

[23] Stosis, T., & Stosis, B. D. (2006). Multifractal Analysis of Human Retinal Vessels. *IEEE Transactions on Medical Imaging*, *25*(8), 1101–1107.

[24] Thomazini, D., Gelfuso, M. V, & Altafim, R. A. C. (2008). Analysis of entropy and fractal dimension to classify the hydrophobicity in polymeric insulators. *Electrical Insulating Materials, 2OO8. (ISEIM 2OO8). International Symposium on*, (2), 279–282. doi:10.1109/ISEIM.2008.4664551

[25] Vasiljevic, J., Reljin, B., Sopta, J., Mijucic, V., Tulic, G., & Reljin, I. (2012). Application of multifractal analysis on microscopic images in the classification of metastatic bone disease. *Biomedical Microdevices*, *l4*, 541–548. doi:22327812

[26] Zaia, A., Eleonori, R., Maponi, P., Rossi, R., & Murri, R. (2006). MR imaging and osteoporosis: Fractal lacunarity analysis of trabecular bone. *IEEE Transactions on Information Technology in Biomedicine*, *lO*(3), 484–489. doi:10.1109/TITB.2006.872078

[27] Zhang, L., Member, S., Wang, L., Member, S., & Lin, W. (2012). Information for Collaborative Image Retrieval. *IEEE Transactions on Image Processing*, *2l*(8), 3707–3720.